NeuroImage: Clinical 33 (2022) 102935

Contents lists available at ScienceDirect

NeuroImage: Clinical

journal homepage: www.elsevier.com/locate/ynicl

Investigating the structure-function relationship of the corticomotor system early after stroke using machine learning

Benjamin Chong [a,b], Alan Wang [b,c], Victor Borges [d], Winston D. Byblow [b,d], P. Alan Barber [a,b], Cathy Stinear [a,b,*]

[a] Department of Medicine, The University of Auckland, New Zealand
[b] Centre for Brain Research, The University of Auckland, New Zealand
[c] Auckland Bioengineering Institute, The University of Auckland, New Zealand
[d] Department of Exercise Sciences, The University of Auckland, New Zealand

ARTICLE INFO

Keywords:
Stroke
Biomarkers
Humans
Magnetic resonance imaging
Transcranial magnetic stimulation
Machine learning

ABSTRACT

Background: Motor outcomes after stroke can be predicted using structural and functional biomarkers of the descending corticomotor pathway, typically measured using magnetic resonance imaging and transcranial magnetic stimulation, respectively. However, the precise structural determinants of intact corticomotor function are unknown. Identifying structure–function links in the corticomotor pathway could provide valuable insight into the mechanisms of post-stroke motor impairment. This study used supervised machine learning to classify upper limb motor evoked potential status using MRI metrics obtained early after stroke.

Methods: Retrospective data from 91 patients (49 women, age 35–97 years) with moderate to severe upper limb weakness within a week after stroke were included in this study. Support vector machine classifiers were trained using metrics from T1- and diffusion-weighted MRI to classify motor evoked potential status, empirically measured using transcranial magnetic stimulation.

Results: Support vector machine classification of motor evoked potential status was 81% accurate, with false positives more common than false negatives. Important structural MRI metrics included diffusion anisotropy asymmetry in the supplementary and pre-supplementary motor tracts, maximum cross-sectional lesion overlap in the sensorimotor tract and ventral premotor tract, and mean diffusivity asymmetry in the posterior limbs of the internal capsule.

Interpretations: MRI measures of corticomotor structure are good but imperfect predictors of corticomotor function. Residual corticomotor function after stroke depends on both the extent of cross-sectional macrostructural tract damage and preservation of white-matter microstructural integrity. Analysing the corticomotor pathway using a multivariable MRI approach across multiple tracts may yield more information than univariate biomarker analyses.

1. Introduction

Recovery from motor impairment after stroke occurs mainly within the first 6 months and has significant inter-individual variability (Prabhakaran et al. 2008). There is a growing interest in the use of biomarker-based approaches to predicting recovery from motor impairment, which can more accurately predict motor recovery and outcomes compared to clinical measures alone (Kim and Winstein 2017, Stinear et al. 2019). Many of the biomarkers that have been explored for predicting motor recovery and outcomes after stroke are derived from neurophysiological or neuroimaging data.

Transcranial magnetic stimulation (TMS) is a non-invasive neurophysiological technique that can be used to assess corticomotor (cortical motor pathway) function. The presence of motor evoked potentials (MEPs) in the paretic upper limb early after stroke in response to TMS of the ipsilesional primary motor cortex is a predictor of good recovery and

Abbreviations: TMS, transcranial magnetic stimulation; MEP, motor evoked potential; MRI, magnetic resonance imaging; SAFE, shoulder abduction finger extension; SVM, support vector machine; SMATT, sensorimotor area tract template; NIHSS, National Institutes of Health Stroke Scale; FM-UE, Fugl-Meyer Upper Extremity.

* Corresponding Author at: Department of Medicine, University of Auckland, Private Bag 92019, Auckland 1142, New Zealand.
E-mail address: c.stinear@auckland.ac.nz (C. Stinear).

https://doi.org/10.1016/j.nicl.2021.102935
Received 26 September 2021; Received in revised form 22 November 2021; Accepted 31 December 2021
Available online 3 January 2022

outcome, even in patients with severe baseline motor deficits (Turton et al. 1996, Hendricks et al. 2002, Nascimbeni et al. 2006, Pizzi et al. 2009, Byblow et al. 2015).

Magnetic resonance imaging (MRI) can be used to obtain a range of structural biomarkers that are associated with upper limb recovery and outcome (Puig et al. 2011, Puig et al. 2013, Feng et al. 2015, Bigourdan et al. 2016, Buch et al. 2016, Puig et al. 2017, Habegger et al. 2018, Boccuni et al. 2019). For example, larger lesion loads (Feng et al. 2015, Boccuni et al. 2019) and lower fractional anisotropies in white matter tracts (Puig et al. 2011, Puig et al. 2013, Buch et al. 2016, Puig et al. 2017) are associated with poorer motor recoveries and outcomes after stroke.

Studies that include both MEP status and structural MRI biomarkers as potential predictors indicate that corticomotor function is more important than corticomotor structure for predicting upper limb outcomes after stroke (Stinear et al. 2012, Stinear et al., 2017a; Stinear et al., 2017b, Buetefisch et al. 2018). Since structure and function are linked, one might wonder if structural information obtained via MRI is able to indicate corticomotor function. Research to date has been unable to classify MEP status accurately using individual structural MRI metrics (Stinear et al., 2017a; Stinear et al., 2017b). However, it may be possible to classify MEP status using multivariable MRI data and supervised machine learning algorithms. Support vector machine is a commonly used machine learning algorithm that solves binary classification problems by calculating a decision boundary. Support vector machine has previously been used to predict future motor outcomes and recovery in the upper limb after stroke using demographic, clinical, imaging, and neurophysiological variables (Lee et al. 2013, Rehme et al. 2015, Guggisberg et al. 2017). Support vector machine can also be used for cross-sectional investigation of corticomotor structure–function relationships by using MRI metrics of corticomotor structure to classify a measure of corticomotor function such as MEP status.

This study aimed to investigate whether structural MRI metrics can be used to classify upper limb MEP status early after stroke using support vector machine, in an analysis of retrospective data. Our hypothesis was that MRI metrics would accurately, but not perfectly, classify MEP status.

2. Methods

2.1. Participants

The study data were drawn from a pool of patients admitted to our hospital between December 2009 and July 2019, who were enrolled in one of five different longitudinal studies (Stinear et al. 2014, Stinear et al., 2017a; Stinear et al., 2017b, Cirillo et al. 2020, two unpublished). Exclusion criteria for all studies were age less than 18 years, bilateral or cerebellar stroke, and impaired cognition or communication precluding informed consent. Shoulder abduction finger extension (SAFE) scores out of 10 were assessed within 5 days of stroke (median 3 days, range 2 – 5 days) using Medical Research Council strength grading (Stinear et al. 2012). Inclusion criteria for the present analysis were ischemic stroke or primary intracerebral haemorrhage with initial moderate to severe upper limb weakness, and MEP status, T1- and diffusion-weighted MRI data available at baseline. Patients with a SAFE score of 5 or more were excluded from the present analysis to produce a balanced sample of MEP positive and MEP negative patients. All studies were approved by the Health and Disability Ethics Committees, and all participants provided written informed consent.

2.2. Transcranial magnetic stimulation

Transcranial magnetic stimulation was used to assess MEP status of the paretic upper limb as early as possible after stroke (median = 9 days, range = 4 – 23 days). Details and video of the most up-to-date protocol are available (Smith et al. 2020). Magnetic stimuli were delivered using a MagStim 200 (MagStim, United Kingdom) connected to a 70 mm figure-of-eight coil, oriented to induce a posterior-anterior current in the hand and arm area of the ipsilesional primary motor cortex. Recording electrodes (Ambu, Denmark, or 3 M, Canada) were placed over the target muscles of the paretic arm in a belly-tendon montage and a reference electrode (3 M, Canada) was placed on the lateral epicondyle of the humerus. One study had extensor carpi radialis as the single target muscle (Stinear et al. 2014), one study had first dorsal interosseous as the single target muscle (Cirillo et al. 2020), and three studies had both extensor carpi radialis and first dorsal interosseous as target muscles (Stinear et al., 2017a; Stinear et al., 2017b, two unpublished). The electromyography signals were sampled at 2 kHz, amplified with a gain of 1000, bandpass filtered between 10 and 1000 Hz or 20 Hz – 1000 Hz using a CED 1902 amplifier and CED Micro1401 mkII data acquisition unit (Cambridge Electronic Design, United Kingdom). The assessor tested various stimulation sites with the coil oriented to induce a posterior-to-anterior current flow in the ipsilesional primary motor cortex. If no MEPs were observed, the stimulation intensity was increased gradually, up to 100% of stimulator output. In three studies, if MEPs were not observable at rest, further stimuli were delivered while the patient attempted voluntary activation of both upper limbs in order to facilitate a response (Stinear et al., 2017a; Stinear et al., 2017b, two unpublished). Patients were categorised as MEP positive if MEPs of any amplitude were consistently observed in any of the target muscles, either at rest or with voluntary activation (Smith et al. 2020).

2.3. Magnetic resonance imaging

T1- and diffusion-weighted MRI were acquired using a Siemens Skyra 3 T or Avanto 1.5 T scanner as early as possible after stroke (median = 10 days, range = 4 – 22 days). The acquisition parameters for each study are provided in Table 1. Lesion masks were manually drawn in participant T1 space by an individual rater (BC) who was blind to stroke severity, MEP status, and clinical outcome. The skull-stripped diffusion-weighted images were corrected for movement, susceptibility-induced distortions, and eddy currents (Andersson et al. 2003, Andersson and Sotiropoulos 2016).

All MRI metrics (except for total lesion volume) were each measured in eight different tracts of interest: seven from the publicly available sensorimotor area tract template (SMATT) (Archer et al. 2018), including primary motor cortex (M1), primary somatosensory cortex (S1), sensorimotor (M1 + S1 combined), ventral premotor cortex, dorsal premotor cortex, supplementary motor area, and pre-supplementary motor area tracts, plus an inhouse template of the posterior limbs of the internal capsule (Stinear et al. 2012). Each participant's T1 was registered to standard 1 mm Montreal Neurological Institute T1 space with a 12 degrees of freedom affine transformation (Jenkinson et al. 2002), followed by a nonlinear transformation (Woolrich et al. 2009). The inverse of these warps was applied to the tracts of interest to transform them into participant T1 space.

An overview of the T1-based MRI metrics is provided in Supplementary Table 1. Weighted lesion load and maximum cross-sectional lesion overlap in each of the tracts of interest, along with total lesion volume, were derived from T1-weighted images. Weighted lesion load was determined by dividing the number of lesion voxels overlapping the tract of interest by the total number of voxels in the tract. Maximum cross-sectional overlap was obtained by calculating the percentage of lesion voxels overlapping the tract of interest for each axial slice and taking the largest value out of all axial slices. Total lesion volume was calculated as the total number of 1 mm isometric voxels in the lesion mask in T1 space.

An overview of the diffusion-based MRI metrics is provided in Supplementary Table 2. Diffusion-weighted images were processed to obtain maps of fractional anisotropy, axial diffusivity, mean diffusivity, radial diffusivity, normalised eigenvalue ratio (Armitage and Bastin 2000), volume fraction (Alexander et al. 2000), scaled relative

Table 1
MRI acquisition parameters for the included studies.

n	Scanner	T1-weighted TR (ms)	TE (ms)	TI (ms)	Flip (°)	Sequence	Diffusion-weighted Resolution (mm)	Flip (°)	TR (ms)	TE (ms)	Volumes
27	Avanto	11	4.94	n/a	15	FLASH3D	1.8 × 1.8 × 3.0	90	6600–6700	101	30 gradients 2 averages 2 b0
39	Avanto	13	4.76	n/a	25	FLASH3D	1.8 × 1.8 × 3.0	90	6500–6700	99–101	30 gradients 2 averages 2 b0
7	Skyra	1900	2.07	900	9	FLASH3D MPRAGE	2.0 × 2.0 × 2.0	78	3600	92	30 gradients 3 b0
3	Skyra	23	2.46	n/a	23	FLASH3D	2.0 × 2.0 × 2.0	78	3600	92.4	64 gradients 8 AP b0 3 PA b0
11*	Avanto	2200	2.97	900	8	FLASH3D MPRAGE	1.8 × 1.8 × 3.0	90	3400	90	64 gradients 2 averages 8 AP b0 3 PA b0
4*	Skyra	2200	2.45	900	8	FLASH3D MPRAGE	2.0 × 2.0 × 2.0	78	3600	92.4	64 gradients 8 AP b0 3 PA b0

* Bottom two rows are different acquisitions from the same study. All T1 images were acquired with 1.0 × 1.0 × 1.0 mm resolution. Diffusion-weighted images were obtained using echo-planar imaging with a b value of 2000 s/mm^2. MRI – magnetic resonance imaging; n – sample size; TR – repetition time; TE – echo time; TI – inversion time; Flip – flip angle; AP – anterior-posterior phase encoding; PA – posterior-anterior phase encoding; FLASH – fast low-angle shot; MPRAGE – magnetisation-prepared rapid gradient echo.

anisotropy (Conturo et al. 1996, Kingsley and Monahan 2005), ultimate anisotropy scaled to the diffusion ellipsoid volume, surface area, or both (UA_{vol}, UA_{surf}, and $UA_{vol,surf}$) (Ulug and van Zijl 1999, Kingsley and Monahan 2005), ellipsoidal area ratio (Xu et al. 2009, Kang et al. 2010), gamma variate anisotropy (Armitage and Bastin 2000), G_{AA} (Pipe and Farthing 2003, Correia et al. 2011), geodesic anisotropy (Batchelor et al. 2005, Correia et al. 2011), and local diffusion homogeneity (Gong and Zang, 2013). The diffusion metric maps were transformed to patient T1 space using a 6 degrees of freedom affine transformation (Jenkinson et al. 2002). The mean values in each tract in patient T1 space were used to calculate asymmetry indices for each diffusion metric using the formula (contra – ipsi) / (contra + ipsi). All image processing was carried out using the FMRIB Software Library 6.0.1 (Woolrich et al. 2009). Calculation of diffusion features was performed using the FMRIB Software Library 6.0.1 and Python 3.7.

2.4. Support vector machine

Support vector machine (SVM) classifiers were trained using Matlab version R2020b (MathWorks, Massachusetts) with linear and radial basis function kernels. The input features included 17 T1-based metrics (weighted lesion loads and maximum cross-sectional lesion overlaps in the 8 tracts of interest, plus total lesion volume), 120 diffusion-based metrics (15 different diffusion tensor metrics in the 8 tracts of interest), and age in years, for a total of 138 input features. The input features were scaled to their respective maximum, and the target variable was empirical MEP status (MEP + or MEP-). The SVM was trained using 10-fold cross-validation, where the data were partitioned randomly into 10 folds, and classifications for each fold were obtained using an SVM model trained on the remaining nine folds. The partitions were stratified by the ground truth and made consistent across all training iterations. The kernel scaling factor and soft margin parameter were optimised using a logarithmic grid-search with 0.001, 0.01, 0.1, 1, 10, 100, and 1000 as possible values. Feature selection was performed using forward selection, where features were iteratively added to the model if they improved the cross-validated model accuracy, until the cross-validation accuracy no longer improved. To evaluate classifier performance, overall cross-validation accuracy, sensitivity, specificity, positive predictive value (PPV), negative predictive value (NPV), and the area under the receiver operating characteristic curve (AUC) were calculated and interpreted as excellent (90 – 100%), good (80 – 90%), moderate (70 – 80%) or poor (50 – 70%).

3. Results

Ninety-one patients were included in this analysis: 84 patients with SAFE scores less than 5, and 7 patients with an unknown SAFE score (Table 2). TMS was used to assess MEP status between 4 and 23 days post-stroke, and MRI was acquired between 5 and 22 days post-stroke. The time between TMS and MRI sessions was up to 9 days, with a median of 2 days. Forty-seven patients were MEP positive, while 44

Table 2
Demographic and clinical characteristics of the study participants.

Age (y)	71 (35 – 97)
Sex (f)	49 (54%)
NIHSS	9 (0 – 21)
SAFE score	1 (0 – 4)
Baseline FM-UE	11 (4 – 53)
MEP+	47 (52%)
Hemisphere (left)	32 (35%)
Dominant side affected	32 (35%)
Handedness (right)	82 (90%)
Haemorrhage	6 (7%)
Thrombolysis	12 (13%)
Thrombectomy	3 (3%)
Previous stroke	9 (10%)
Smoker	7 (8%)
Diabetes	21 (23%)
Hypertension	53 (58%)
Dyslipidaemia	38 (42%)
Atrial fibrillation	18 (20%)
Previous cardiac event	22 (24%)
TMS day	8 (4 – 23)
MRI day	11 (5 – 22)
Days between TMS and MRI	2 (-9 – 9)

Values are median (range), or n (%).
NIHSS – National Institutes of Health Stroke Scale; SAFE – shoulder abduction finger extension; FM-UE – Fugl-Meyer Upper Extremity; MEP+ – motor evoked potential present; TMS – transcranial magnetic stimulation.

patients were MEP negative. An overlay of the lesion masks is provided in Fig. 1.

The radial basis function kernel SVM correctly classified MEP status for 74 out of 91 patients, with a cross-validation accuracy of 81.3%. There were three final model solutions, all of which included UA_{surf} asymmetry in the supplementary motor tract and volume fraction asymmetry in the pre-supplementary motor tract as model features. Model 1 also included sensorimotor tract maximum cross-sectional lesion overlap. Model 2 included ventral premotor tract maximum cross-sectional overlap. Model 3 included mean diffusivity asymmetry in the posterior limbs of the internal capsule. Optimum hyperparameters were a kernel scaling factor of 10 and a soft margin parameter of 1000 for all three model solutions.

All three models had good AUC (Fig. 2) and sensitivity, moderate specificity and NPV, while PPV ranged from moderate to borderline moderate/good (Table 3). Model 3 had the highest AUC of 83.4%. Of the incorrect predictions, false positives were more common than false negatives (Table 4). Furthermore, eight of the false positives and three of the false negatives were consistent throughout all three models, indicating that the incorrect classifications were often for the same patients. When stratifying patients by time between TMS and MRI (0 – 3 days versus 4 – 9 days), Model 1 performed better for patients who had intervals of 0 – 3 days, while Model 3 performed better for patients with intervals of 4 – 9 days, and Model 2 performed similarly regardless of interval between TMS and MRI (Supplementary Table 3). Linear kernel SVM did not perform as well, achieving a maximum cross-validation accuracy of 79.1%. There were no obvious clinical differences between the patients who were correctly or incorrectly classified for either model.

4. Discussion

This study investigated whether structural data obtained from T1- and diffusion-weighted MRI could be used to classify MEP status, a TMS measure of corticomotor function, in patients early after stroke. This is the first study to use machine learning to classify MEP status after stroke, and one of few studies that use multivariable MRI data for classification after stroke. To date, most studies that use MRI metrics for regression or classification problems do so using univariate approaches.

While a previous study was unable to predict MEP status using individual MRI metrics (Stinear et al., 2017a; Stinear et al., 2017b), the present study demonstrates that an SVM approach using multiple structural MRI metrics can accurately predict MEP status. This indicates that corticomotor structure and function are significantly interrelated, and that structure can predict function to an extent. The two structural metrics that featured in all final SVM models were supplementary motor tract UA_{surf} asymmetry and pre-supplementary motor tract volume fraction asymmetry. Additional features included either maximum cross-sectional lesion overlap in the sensorimotor (Model 1) or ventral premotor tracts (Model 2), or mean diffusivity asymmetry in the posterior limbs of the interior capsule (Model 3).

Interestingly, maximum cross-sectional lesion overlap was included in the final feature combinations, while weighted lesion load was not.

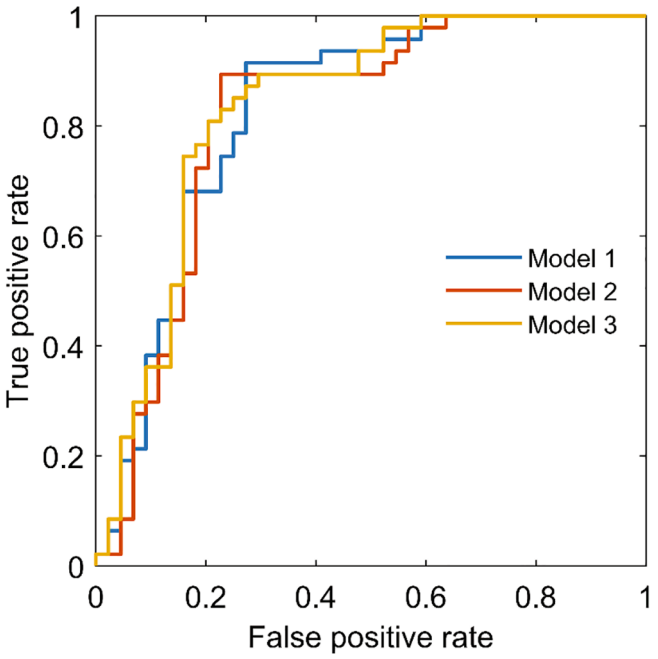

Fig. 2. Receiver operating characteristic curves for motor evoked potential classification.

Table 3
Performance measures for final SVM models.

	Accuracy	Sens	Spec	PPV	NPV	AUC
Model 1	81.3	89.4	72.7	77.8	86.5	82.8
Model 2	81.3	85.1	77.3	80.0	82.9	81.8
Model 3	81.3	87.2	75.0	78.8	84.6	83.4

SVM – support vector machine; sens – sensitivity; spec – specificity; PPV – positive predictive value; NPV – negative predictive value; AUC – area under the receiver operating characteristic curve. Model 1 features: UA_{surf} asymmetry in the supplementary motor tract, volume fraction asymmetry in the pre-supplementary motor tract, and sensorimotor tract maximum cross-sectional overlap. Model 2 features: UA_{surf} asymmetry in the supplementary motor tract, volume fraction asymmetry in the pre-supplementary motor tract, and ventral premotor tract maximum cross-sectional overlap. Model 3 features: UA_{surf} asymmetry in the supplementary motor tract, volume fraction asymmetry in the pre-supplementary motor tract, and mean diffusivity asymmetry in the posterior limbs of the internal capsule.

Both of these metrics measure the macrostructural overlap between the lesion and the tract of interest, with a key difference; maximum cross-sectional lesion overlap is dependent on the single axial slice with the greatest lesion overlap, while weighted lesion load reflects the overall extent of damage to the tract along its full length. Our results indicate that the maximum severity of cross-sectional tract damage may be more relevant than the overall extent of tract damage for corticomotor

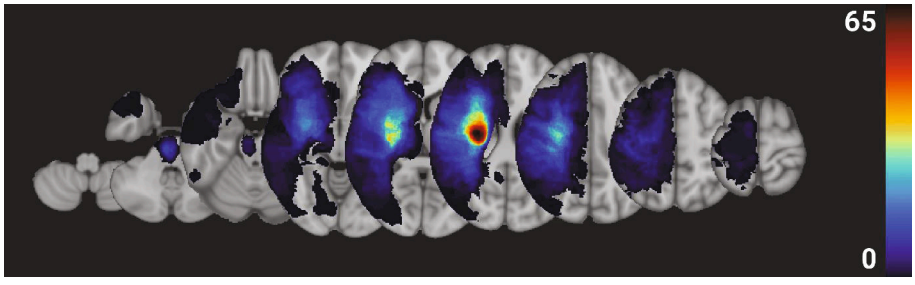

Fig. 1. Lesion map of all patients (flipped to left hemisphere) in standard T1 1 mm space.

Table 4
Cross-tabulation of predicted versus actual MEP status.

	Ground truth MEP+	MEP-
Model 1 predictions		
MEP+	42	12
MEP-	5	32
Model 2 predictions		
MEP+	40	10
MEP-	7	34
Model 3 predictions		
MEP+	41	11
MEP-	6	33

MEP – motor evoked potential.

functional integrity. This can be explained by the fact that a lesion across the width of a tract will affect a larger number of axons than a lesion of the same size along the length of the tract, due to the longitudinal arrangement of axons.

Of the final model features derived from diffusion-weighted imaging, UA_{surf} and volume fraction are measures of diffusion tensor anisotropy, while mean diffusivity is a measure of the overall extent of diffusion. All three of these metrics are sensitive to white matter microstructure such as axonal membranes and myelin, a general feature of diffusion tensor metrics (Sen and Basser 2005, Schmierer et al. 2008). The strong presence of these diffusion metrics in the final SVM models emphasises that the retention of corticomotor function after stroke is dependent on the preservation of white matter microstructural integrity. Age did not survive feature selection, which suggests that the MRI metrics important for determining corticomotor function are not dependent on age.

The importance of the supplementary, pre-supplementary, and premotor tract structural integrity towards corticomotor function is an interesting finding, considering that MEPs have long been known to arise from the primary motor cortex (Hallett 2007). However, the results of the present study do not necessarily mean that MEPs arise from non-primary motor tracts, as there are structural overlaps between each of these tracts and the M1 tract, particularly at the level of and inferior to the internal capsule. The various tract combinations identified in this study may have produced a fuzzy delineation of the M1 tract that better accounted for inter-individual anatomical variability compared to a standalone M1 tract template.

We note that the specific feature combinations identified in this study are not the key takeaway from this research, as future studies applying these methods to a new dataset may identify different combinations of tracts and metrics. Instead, the present study indicates that analysing the corticomotor pathway using a multivariable approach across multiple different tracts may be better than measuring an individual MRI biomarker from a single region of interest. The combination of both T1- and diffusion-based MRI metrics allows the SVM to account for both macro- and microstructural aspects of corticomotor pathway injury, which a univariate MRI biomarker analysis cannot. Furthermore, including measures across multiple different overlapping tracts may help to account for inter-individual anatomical variability and slight variations in tract fitting.

The SVM could not correctly predict MEP status for 19% of patients. Prediction errors included both false positives and false negatives, indicating that some patients with relatively high corticomotor structural integrity can be MEP negative, and some patients with relatively poor corticomotor structural integrity can be MEP positive, of which the former was more common. This finding indicates that there are aspects of corticomotor function that cannot be predicted by the MRI measures of corticomotor structure examined in this study. Other non-structural factors such as corticomotor excitability and tonic inhibition may also influence the function of structurally intact corticomotor tracts (Cirillo et al. 2020).

A limitation of the present study is the time between TMS and MRI assessments, which varied between participants. On average, there was a 2-day gap between TMS and MRI assessments. In some patients, TMS preceded MRI by up to 9 days, while in others, MRI preceded TMS by up to 9 days. More closely spaced assessments could reduce the confounding effect of time and improve prediction accuracies. However, while Model 3 performed better for patients with small time gaps (0 – 3 days), Model 1 was more accurate for patients with larger gaps (4 – 9 days), and Model 2 accuracy was unaffected by TMS-MRI time gap.

Another limitation is that the SMATT template tracts were developed from scans in healthy young adults rather than people after stroke (Archer et al. 2018). Our dataset included MRI scans from stroke patients with varied acquisition parameters, such as magnetic field strength, pulse timing, image resolution, and gradient directions. Importantly however, all the imaging metrics in this study are independent of image intensity and therefore robust against intensity variations between different scanning acquisitions. The variety of acquisitions increases the generalisability of this work to a wider range of clinical settings where scanning protocols may differ.

In conclusion, this study demonstrates that structural MRI metrics can be used in combination with SVM to accurately classify MEP status in stroke patients with moderate to severe upper limb weakness. Residual corticomotor function after stroke appears to be dependent on both the extent of macrostructural cross-sectional tract damage and preservation of white matter microstructural integrity. Analysing the corticomotor pathway using a multivariable MRI approach in combination with machine learning can provide more information than univariate biomarker analysis, as the former can account for different aspects of structural damage and inter-individual anatomical variability. The structural determinants of corticomotor function after stroke are still not fully understood and could see further investigation. Future research could also use multivariable MRI data in combination with machine learning techniques as an alternative to single biomarker analyses.

CRediT authorship contribution statement

Benjamin Chong: Conceptualization, Methodology, Software, Formal analysis, Investigation, Writing – original draft, Writing – review & editing. **Alan Wang:** Conceptualization, Methodology, Software, Writing – review & editing, Supervision. **Victor Borges:** Software, Formal analysis, Writing – review & editing. **Winston D. Byblow:** Writing – review & editing, Supervision, Funding acquisition. **P. Alan Barber:** Writing – review & editing, Funding acquisition. **Cathy Stinear:** Conceptualization, Methodology, Resources, Writing – review & editing, Supervision, Project administration, Funding acquisition.

Declaration of Competing Interest

The authors declare that they have no known competing financial interests or personal relationships that could have appeared to influence the work reported in this paper.

Acknowledgements

The authors acknowledge the researchers and participants of the included studies, in particular Dr. Marie-Claire Smith, Dr. Suzanne Ackerley, and Christine Mangold.

Funding

This work was supported by the Health Research Council of New Zealand [grant numbers 09/164R, 11/270, 14/136]; and the Neurological Foundation of New Zealand [grant numbers 1640-PG, 1735-PG].

Appendix A. Supplementary data

Supplementary data to this article can be found online at https://doi.org/10.1016/j.nicl.2021.102935.

References

Alexander, A.L., Hasan, K., Kindlmann, G., Parker, D.L., Tsuruda, J.S., 2000. A geometric analysis of diffusion tensor measurements of the human brain. Magn Reson Med. 44 (2), 283–291. https://doi.org/10.1002/1522-2594(200008)44:2<283::aid-mrm16>3.0.co;2-v.

Andersson, J.L., Skare, S., Ashburner, J., 2003. How to correct susceptibility distortions in spin-echo echo-planar images: application to diffusion tensor imaging. NeuroImage. 20 (2), 870–888. https://doi.org/10.1016/s1053-8119(03)00336-7.

Andersson, J.L.R., Sotiropoulos, S.N., 2016. An integrated approach to correction for off-resonance effects and subject movement in diffusion MR imaging. NeuroImage. 125, 1063–1078. https://doi.org/10.1016/j.neuroimage.2015.10.019.

Archer, D.B., Vaillancourt, D.E., Coombes, S.A., 2018. A Template and Probabilistic Atlas of the Human Sensorimotor Tracts using Diffusion MRI. Cereb Cortex. 28 (5), 1685–1699. https://doi.org/10.1093/cercor/bhx066.

Armitage, P.A., Bastin, M.E., 2000. Selecting an appropriate anisotropy index for displaying diffusion tensor imaging data with improved contrast and sensitivity. Magn Reson Med. 44 (1), 117–121. https://doi.org/10.1002/1522-2594(200007)44:1<117::aid-mrm17>3.0.co;2-d.

Batchelor, P.G., Moakher, M., Atkinson, D., Calamante, F., Connelly, A., 2005. A rigorous framework for diffusion tensor calculus. Magn Reson Med. 53 (1), 221–225. https://doi.org/10.1002/mrm.20334.

Bigourdan, A., Munsch, F., Coupe, P., Guttmann, C.R., Sagnier, S., Renou, P., Debruxelles, S., Poli, M., Dousset, V., Sibon, I., Tourdias, T., 2016. Early Fiber Number Ratio Is a Surrogate of Corticospinal Tract Integrity and Predicts Motor Recovery After Stroke. Stroke. 47 (4), 1053–1059. https://doi.org/10.1161/strokeaha.115.011576.

Boccuni, L., Meyer, S., D'Cruz, N., Kessner, S.S., Marinelli, L., Trompetto, C., Peeters, A., Van Pesch, V., Duprez, T., Sunaert, S., Feys, H., Thijs, V., Nieuwboer, A., Verheyden, G., 2019. Premotor dorsal white matter integrity for the prediction of upper limb motor impairment after stroke. Sci Rep. 9 (1), 19712. https://doi.org/10.1038/s41598-019-56334-w.

Buch, E.R., Rizk, S., Nicolo, P., Cohen, L.G., Schnider, A., Guggisberg, A.G., 2016. Predicting motor improvement after stroke with clinical assessment and diffusion tensor imaging. Neurol. 86 (20), 1924–1925. https://doi.org/10.1212/wnl.0000000000002675.

Buetefisch, C.M., Revill, K.P., Haut, M.W., Kowalski, G.M., Wischnewski, M., Pifer, M., Belagaje, S.R., Nahab, F., Cobia, D.J., Hu, X., Drake, D., Hobbs, G., 2018. Abnormally reduced primary motor cortex output is related to impaired hand function in chronic stroke. J Neurophysiol. 120 (4), 1680–1694. https://doi.org/10.1152/jn.00715.2017.

Byblow, W.D., Stinear, C.M., Barber, P.A., Petoe, M.A., Ackerley, S.J., 2015. Proportional recovery after stroke depends on corticomotor integrity. Ann Neurol. 78 (6), 848–859. https://doi.org/10.1002/ana.24472.

Cirillo, J., Mooney, R.A., Ackerley, S.J., Barber, P.A., Borges, V.M., Clarkson, A.N., Mangold, C., Ren, A., Smith, M.-C., Stinear, C.M., Byblow, W.D., 2020. Neurochemical balance and inhibition at the sub-acute stage after stroke. J Neurophysiol 123 (5), 1775–1790. https://doi.org/10.1152/jn.00561.2019.

Conturo, T.E., McKinstry, R.C., Akbudak, E., Robinson, B.H., 1996. Encoding of anisotropic diffusion with tetrahedral gradients: a general mathematical diffusion formalism and experimental results. Magn Reson Med. 35 (3), 399–412. https://doi.org/10.1002/mrm.1910350319.

Correia, M.M., Newcombe, V.F.J., Williams, G.B., 2011. Contrast-to-noise ratios for indices of anisotropy obtained from diffusion MRI: A study with standard clinical b-values at 3T. NeuroImage. 57 (3), 1103–1115. https://doi.org/10.1016/j.neuroimage.2011.03.004.

Feng, W., Wang, J., Chhatbar, P.Y., Doughty, C., Landsittel, D., Lioutas, V.A., Kautz, S.A., Schlaug, G., 2015. Corticospinal tract lesion load: An imaging biomarker for stroke motor outcomes. Ann Neurol. 78 (6), 860–870. https://doi.org/10.1002/ana.24510.

Gong, G., Zang, Y.-F., 2013. Local diffusion homogeneity (LDH): an inter-voxel diffusion MRI metric for assessing inter-subject white matter variability. PLoS One. 8 (6), e66366. https://doi.org/10.1371/journal.pone.0066366.

Guggisberg, A.G., Nicolo, P., Cohen, L.G., Schnider, A., Buch, E.R., 2017. Longitudinal Structural and Functional Differences Between Proportional and Poor Motor Recovery After Stroke. Neurorehabil Neural Repair. 31 (12), 1029–1041. https://doi.org/10.1177/1545968317740634.

Habegger, S., Wiest, R., Weder, B.J., Mordasini, P., Gralla, J., Hani, L., Jung, S., Reyes, M., McKinley, R., 2018. Relating Acute Lesion Loads to Chronic Outcome in Ischemic Stroke-An Exploratory Comparison of Mismatch Patterns and Predictive Modeling. Front Neurol. 9, 737. https://doi.org/10.3389/fneur.2018.00737.

Hallett, M., 2007. Transcranial magnetic stimulation: a primer. Neuron. 55 (2), 187–199. https://doi.org/10.1016/j.neuron.2007.06.026.

Hendricks, H.T., Zwarts, M.J., Plat, E.F., van Limbeek, J., 2002. Systematic review for the early prediction of motor and functional outcome after stroke by using motor-evoked potentials. Arch Phys Med Rehabil. 83 (9), 1303–1308. https://doi.org/10.1053/apmr.2002.34284.

Jenkinson, M., Bannister, P., Brady, M., Smith, S., 2002. Improved optimization for the robust and accurate linear registration and motion correction of brain images. NeuroImage. 17 (2), 825–841. https://doi.org/10.1016/s1053-8119(02)91132-8.

Kang, X., Herron, T.J., Woods, D.L., 2010. Validation of the anisotropy index ellipsoidal area ratio in diffusion tensor imaging. Magn Reson Imaging. 28 (4), 546–556. https://doi.org/10.1016/j.mri.2009.12.015.

Kim, B., Winstein, C., 2017. Can Neurological Biomarkers of Brain Impairment Be Used to Predict Poststroke Motor Recovery? A Systematic Review. Neurorehabil Neural Repair. 31 (1), 3–24. https://doi.org/10.1177/1545968316662708.

Kingsley, P.B., Monahan, W.G., 2005. Contrast-to-noise ratios of diffusion anisotropy indices. Magn Reson Med. 53 (4), 911–918. https://doi.org/10.1002/mrm.20433.

Lee, J.D., Chang, T.C., Yang, S.T., Huang, C.H., Wu, C.Y., 2013. The potential predictors of motor performance outcomes after rehabilitation for patients with stroke. Applied Mechanics and Materials. 284–287, 1656–1660. https://doi.org/10.4028/www.scientific.net/AMM.284-287.1656.

Nascimbeni, A., Gaffuri, A., Imazio, P., 2006. Motor evoked potentials: Prognostic value in motor recovery after stroke. Funct Neurol. 21 (4), 199–203.

Pipe, J.G., Farthing, V.G., 2003. A correlative measure for processing multiangle diffusion-weighted images. Magn Reson Med. 49 (3), 536–542. https://doi.org/10.1002/mrm.10399.

Pizzi, A., Carrai, R., Falsini, C., Martini, M., Verdesca, S., Grippo, A., 2009. Prognostic value of motor evoked potentials in motor function recovery of upper limb after stroke. J Rehabil Med. 41 (8), 654–660. https://doi.org/10.2340/16501977-0389.

Prabhakaran, S., Zarahn, E., Riley, C., Speizer, A., Chong, J.Y., Lazar, R.M., Marshall, R. S., Krakauer, J.W., 2008. Inter-individual variability in the capacity for motor recovery after ischemic stroke. Neurorehabil Neural Repair. 22 (1), 64–71. https://doi.org/10.1177/1545968307305302.

Puig, J., Blasco, G., Daunis, I.E.J., Thomalla, G., Castellanos, M., Figueras, J., Remollo, S., van Eendenburg, C., Sanchez-Gonzalez, J., Serena, J., Pedraza, S., 2013. Decreased corticospinal tract fractional anisotropy predicts long-term motor outcome after stroke. Stroke. 44 (7), 2016–2018. https://doi.org/10.1161/strokeaha.111.000382.

Puig, J., Blasco, G., Schlaug, G., Stinear, C.M., Daunis, I.E.P., Biarnes, C., Figueras, J., Serena, J., Hernandez-Perez, M., Alberich-Bayarri, A., Castellanos, M., Liebeskind, D. S., Demchuk, A.M., Menon, B.K., Thomalla, G., Nael, K., Wintermark, M., Pedraza, S., 2017. Diffusion tensor imaging as a prognostic biomarker for motor recovery and rehabilitation after stroke. Neuroradiol. 59 (4), 343–351. https://doi.org/10.1007/s00234-017-1816-0.

Puig, J., Pedraza, S., Blasco, G., Daunis, I.E.J., Prados, F., Remollo, S., Prats-Galino, A., Soria, G., Boada, I., Castellanos, M., Serena, J., 2011. Acute damage to the posterior limb of the internal capsule on diffusion tensor tractography as an early imaging predictor of motor outcome after stroke. Am J Neuroradiol. 32 (5), 857–863. https://doi.org/10.3174/ajnr.A2400.

Rehme, A.K., Volz, L.J., Feis, D.L., Eickhoff, S.B., Fink, G.R., Grefkes, C., 2015. Individual prediction of chronic motor outcome in the acute post-stroke stage: Behavioral parameters versus functional imaging. Hum Brain Mapp. 36 (11), 4553–4565. https://doi.org/10.1002/hbm.22936.

Schmierer, K., Wheeler-Kingshott, C.A.M., Tozer, D.J., Boulby, P.A., Parkes, H.G., Yousry, T.A., Scaravilli, F., Barker, G.J., Tofts, P.S., Miller, D.H., 2008. Quantitative magnetic resonance of postmortem multiple sclerosis brain before and after fixation. Magn Reson Med. 59 (2), 268–277. https://doi.org/10.1002/mrm.21487.

Sen, P.N., Basser, P.J., 2005. A model for diffusion in white matter in the brain. Biophysical journal. 89 (5), 2927–2938. https://doi.org/10.1529/biophysj.105.063016.

Smith, M.C., Ackerley, S.J., Monigatti, E.J., Scrivener, B.J., Stinear, C.M., 2020. Determining the Functional Status of the Corticospinal Tract Within One Week of Stroke. J Vis Exp. 156 https://doi.org/10.3791/60665.

Stinear, C.M., Barber, P.A., Petoe, M., Anwar, S., Byblow, W.D., 2012. The PREP algorithm predicts potential for upper limb recovery after stroke. Brain. 135 (Pt 8), 2527–2535. https://doi.org/10.1093/brain/aws146.

Stinear, C.M., Byblow, W.D., Ackerley, S.J., Barber, P.A., Smith, M.C., 2017a. Predicting Recovery Potential for Individual Stroke Patients Increases Rehabilitation Efficiency. Stroke. 48 (4), 1011–1019. https://doi.org/10.1161/strokeaha.116.015790.

Stinear, C.M., Byblow, W.D., Ackerley, S.J., Smith, M.-C., Borges, V.M., Barber, P.A., 2017b. PREP2: A biomarker-based algorithm for predicting upper limb function after stroke. Ann Clin Transl Neurol. 4 (11), 811–820. https://doi.org/10.1002/acn3.488.

Stinear, C.M., Petoe, M.A., Anwar, S., Barber, P.A., Byblow, W.D., 2014. Bilateral priming accelerates recovery of upper limb function after stroke: a randomized controlled trial. Stroke. 45 (1), 205–210. https://doi.org/10.1161/strokeaha.113.003537.

Stinear, C.M., Smith, M.C., Byblow, W.D., 2019. Prediction Tools for Stroke Rehabilitation. Stroke. 50 (11), 3314–3322. https://doi.org/10.1161/strokeaha.119.025696.

Turton, A., Wroe, S., Trepte, N., Fraser, C., Lemon, R.N., 1996. Contralateral and ipsilateral EMG responses to transcranial magnetic stimulation during recovery of arm and hand function after stroke. Electroencephalogr Clin Neurophysiol. 101 (4), 316–328. https://doi.org/10.1016/0924-980X(96)95560-5.

Ulug, A.M., van Zijl, P.C., 1999. Orientation-independent diffusion imaging without tensor diagonalization: anisotropy definitions based on physical attributes of the diffusion ellipsoid. J Magn Reson Imaging. 9 (6), 804–813. https://doi.org/10.1002/(sici)1522-2586(199906)9:6<804::aid-jmri7>3.0.co;2-b.

Woolrich, M.W., Jbabdi, S., Patenaude, B., Chappell, M., Makni, S., Behrens, T., Beckmann, C., Jenkinson, M., Smith, S.M., 2009. Bayesian analysis of neuroimaging data in FSL. NeuroImage. 45 (1 Suppl), S173–S186. https://doi.org/10.1016/j.neuroimage.2008.10.055.

Xu, D., Cui, J., Bansal, R., Hao, X., Liu, J., Chen, W., Peterson, B.S., 2009. The ellipsoidal area ratio: an alternative anisotropy index for diffusion tensor imaging. Magn Reson Imaging. 27 (3), 311–323. https://doi.org/10.1016/j.mri.2008.07.018.